16th World Congress in Computational Mechanics (WCCM)
21-26 July 2024, Vancouver, Canada
A. Korobenko, M. Laforest, S. Prudhomme, R. Vaziri (Eds)

NUMERICAL SIMULATIONS OF ORIGAMI-BASED FOLDED CARBON-REINFORCED CONCRETE SHELLS

SPARTALI H.[1] GOMES C. G.[1] MESTER L.[2] KIKIS G.[2] KLARMANN S.[2] KLINKEL S.[2] AND CHUDOBA R.[1]

[1] Insitute of Structural Concrete, RWTH Aachen University
Mies-van-der-Rohe Str. 1, 52074 Aachen, Germany
hspartali@imb.rwth-aachen.de

[2] Institute of Structural Analysis and Dynamics, RWTH Aachen University
Mies-van-der-Rohe Str. 1, 52074 Aachen, Germany

Key words: textile reinforced concrete, carbon concrete, thin-walled elements, folded shells, nonlinear numerical modeling of CRC structures

Abstract. The advantages of carbon-reinforced concrete (CRC) over traditional concrete elements reinforced with steel, including high strength, low weight, and corrosion resistance, make it a promising material for thin, efficient, and more sustainable designs. As the demand for less CO_2-intensive materials such as concrete grows, a shift from simple massive elements to thin-walled elements with complex geometries is becoming increasingly necessary. However, to seek optimal design variants, efficient nonlinear numerical calculations that provide reasonable predictions of the structural behavior, including the stress-redistribution process and the failure mechanisms are essential. This paper presents FEM simulations of origami-based folded CRC shells that were experimentally investigated in a previous study. Two FEM modeling approaches were used, employing a smeared and a discrete representation of the carbon reinforcement. For both approaches a damage plasticity model for the concrete has been used. The load-deflection response from the discrete approach closely matches the experimentally obtained curves. Despite an overestimation of the load capacity, the computationally less expensive smeared FEM model qualitatively reproduces the structural response and the correct failure mechanism. Therefore, the quality of the results obtained from the smeared model is sufficient to determine preferable design variants in a typical design scenario. This is necessary to provide a deeper understanding of the structural behavior of these folded elements and to facilitate the sustainable design and application of thin-walled CRC elements in the future.

1 INTRODUCTION

The construction industry, a major source of CO_2 emissions, requires novel sustainable approaches spanning the entire construction process. Despite the significant impact of structural design on material waste, the employment of traditional inefficient designs and construction

techniques is still the common practice today [1]. However, the advances on high-performance corrosion-resistant reinforcements like carbon fiber reinforced polymers (CFRP) enables the design of more efficient thin-walled structures [7][9][10][12]. Yet, the development of adaptive design strategies for these structural elements is still in its infancy and lacks customizable, material-efficient, and practical design methodologies.

One promising design concept is based on the principles of structural engineering with the art of origami, specifically the waterbomb pattern. Originating from the Japanese paper-folding tradition, the inherent form flexibility and structural integrity of the waterbomb pattern when tessellated and folded provides a compelling framework for creating thin-walled carbon concrete elements [5]. By employing the flat foldability and kinematics of waterbomb tessellations, a wide range of different three-dimensional structures can be efficiently produced, paving the way for a reusable, customizable, and modular production process [12].

In the pursuit of optimal design solutions, this paper introduces nonlinear FEM calculations employing two different modeling approaches for origami-based carbon reinforced concrete shells. First, the geometry of the folded waterbomb shells is described, in addition to the loading type and boundary conditions, followed by the material assumptions for the numerical simulation. Then, the simulation results are presented and discussed in detail, and the conclusions are provided in a final section.

The presented modeling results are part of a wide range of experimental and numerical investigations aimed at providing a comprehensive framework for the analysis, design, and fabrication of folded material-efficient textile reinforced concrete elements. In particular, they aim to support the identification of optimal structural forms from the wide range of structural geometries obtainable by varying the parameters of the origami waterbomb pattern.

2 METHODOLOGY

2.1 Folded shell geometries

The geometry of the studied folded shell are obtained based on the analytical solution of the symmetrically folded waterbomb pattern proposed by [5]. Given a set of design parameters of the basic component of the waterbomb pattern, i.e., the waterbomb cell (see Fig. 1), which are the lengths a, b, and c, in addition to a folding angle γ, the analytical solution describes the resulting 3D folded geometry. Using different combinations of these design parameters, various folded geometrical forms with different waterbomb cell densities are obtainable for a unique folded target geometry. In this case, a shell geometry based on a waterbomb pattern with two cells along the shell span was chosen, as shown in Fig. 1. Multiple folded shells with this geometry, which are numerically modeled in this study, have also been produced and experimentally tested in [11]. All shells have an effective span of 180 cm and a height of 30 cm in the final folded state. The base waterbomb cell, the folding pattern, and the final geometry of the folded shells are illustrated in Fig. 1. In addition, the figure shows the two cross-sectional variants investigated, namely 1 cm and 2 cm thick sections with one and two carbon textile layers, respectively. In analogy to [11], the shells are denoted in the format "S#-TxRy", where

(#) is the shell number and (x), (y) are replaced by the shell thickness in cm and the number of reinforcement layers, respectively. The five experimentally tested shells with the two mentioned cross-section variants are denoted as S1-T1R1, S2-T1R1, S3-T1R1, S4-T2R2, and S5-T2R2.

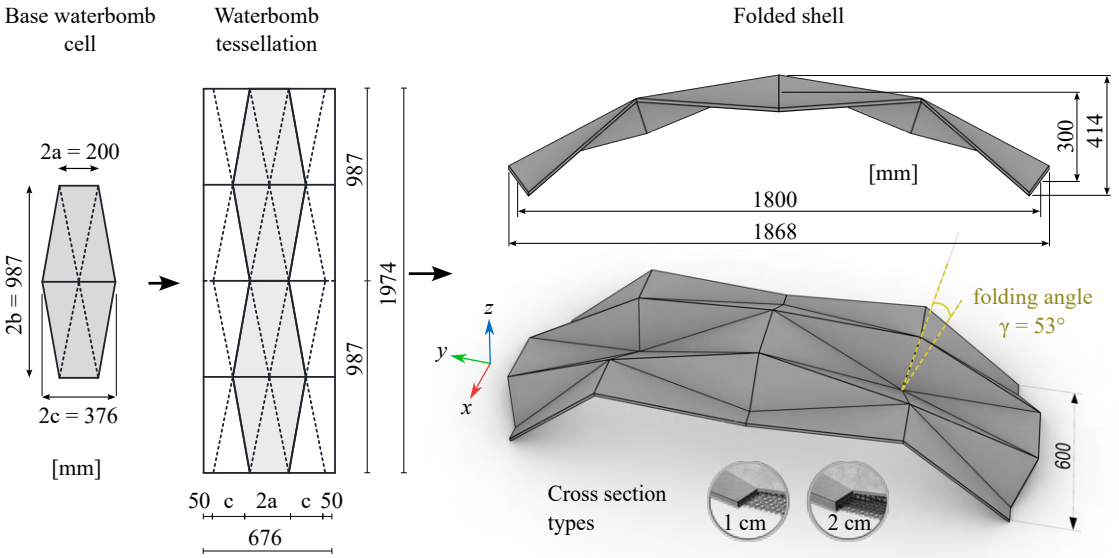

Figure 1: Folding pattern and final folded form of the modeled shells.

2.2 Loading and boundary conditions

Due to the symmetric properties of the shell geometry and the associated boundary conditions, the numerical model was reduced to one half of the shell by introducing displacement constraints on the symmetry plane at the midspan of the shell. Furthermore, the load is applied as a displacement of u_z = -30 mm in 50 steps on the horizontal edge at midspan, analogous to the experiments. In case a structural failure occurs before the full loading process of 50 steps, the calculation is interrupted.

For better comparability of the numerical and experimental results, the boundary conditions must closely reflect the observations from the experimental tests. Although a fixed support configuration at the ends of the shells was intended during the tests, a small horizontal support displacement of 1-4 mm at shell ends was unavoidable as reported in [11]. This displacement has a significant influence on the structural behavior due to the high horizontal reactions of the shells with low curvature. Therefore, it was taken into account in the numerical model by applying a spring in the y-direction at the supported edge of the shell.

The springs' stiffness k_s = 26.9 N/mm^2 for the 1 cm and k_s = 26 N/mm^2 for the 2 cm thick shell models are obtained experimentally based on the respective maximum load capacity and

the horizontal displacement of the support in [11].

2.3 Model discretization, constitutive laws and material properties

Two modeling approaches have been used to build the FE models, which aim to provide a computationally efficient numerical solution to assist in the identification of highly efficient folded geometries. These modeling approaches are labeled "FEM discrete" and "FEM smeared" in the following and are carried out on the commercial software ATENA [3]. The "FEM discrete" model uses 3D solid curvilinear shell elements with 12 nodes for the concrete discretization and truss elements for the textile reinforcement roving discretization. The concrete material law considers the classical orthotropic smeared crack formulation for fracture in tension and the three-parameter Menétrey-William failure surface for hardening/softening plasticity in compression, refer to [4] for a detailed description of the models. For the discrete FEM, two different bond laws between the textile rovings and the concrete have been investigated, a perfect bond law (the default case) and a simplified multilinear law to closely capture the bond behavior of the used unimpregnated carbon rovings. This multilinear law is based on the data provided in [13] for a similar type of plain carbon roving with a bond strength of 5.75 MPa assuming a roving perimeter of 4 mm.

The FEM smeared model considers a 3D surface representation of the shell geometry and 2D curvilinear triangular shell elements with 6 nodes for the discretization. The material law applied in this case is an adaptation of the fracture-elastic concrete material used in the "FEM discrete" approach to consider the textile reinforcement in a smeared manner, based on the Aveston-Cooper-Kelly (ACK) model proposed by [2]. The compressive behavior of the fracture-elastic concrete model remains unchanged, but the tensile behavior is adjusted to reproduce the response of the carbon-reinforced concrete composite using the ACK model.

The mechanical properties of the concrete and reinforcement for the FE models are given in Table. 1. These are taken similar to the data reported in [11]. However, the tensile strength of the carbon rovings is obtained from new tensile tests performed on rovings identical to those used for the tests in [11]. The carbon textile reinforcement consists of an equidistant grid of rovings with a spacing of 10 mm in both directions and a cross-sectional area of A_{rov} = 0.94 mm^2.

Table 1: Mechanical properties of the concrete and the carbon fiber reinforcement

Concrete		Carbon fiber reinforcement	
$\mathrm{E_{cm}}$	24 360 MPa	$\mathrm{E_f}$	123 880 MPa [6]
f_{cm}	68 MPa	f_{fu}	1150 MPa
f_{ctm}	3 MPa		

3 RESULTS AND DISCUSSION

3.1 Comparison between 2D and 3D shell elements

The 2D shell elements presents a higher computational efficiency compared to the 3D shell element. However, it should be assured that the reduction from a 3D to a 2D element idealization in the case of the smeared FEM model does not significantly affect the model's results. Therefore, two cases of the 1 cm thick shell were simulated, one with a fixed and one with a spring boundary condition in the y-direction, both cases with the 2D and 3D elements and the smeared material representation. To assess the equivalence of the models, the load-deflection curves are evaluated and plotted in Fig. 2 showing analogous results. Thus, confirming that the reduction to 2D shell elements in the case of the smeared FEM approach has a negligible effect on the results. It should be noted that in the case of the discrete FEM model, 3D shell elements are required to accommodate the discrete reinforcement and to properly capture the bond effect.

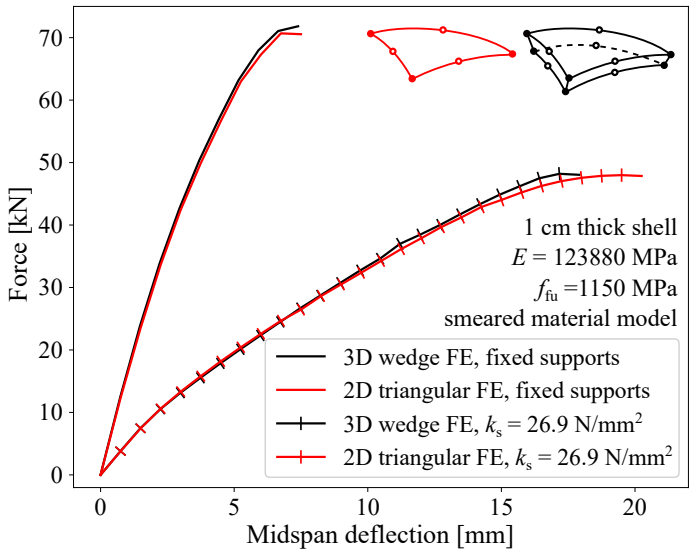

Figure 2: Comparison of the results of the smeared FEM model using two different shell element types,i.e., 3D wedge elements and 2D triangular elements

3.2 Effect of support stiffness and FEM modeling approach

The stiffness of the supports at both shell ends in the y-direction has a significant influence on the structural behavior as a result of the small curvature of the shell geometry and consequently the larger horizontal reaction. This influence was evaluated by calculating both shell variants, i.e. 1 cm and 2 cm thick shells, using both FEM approaches with varying stiffness of the imposed springs (k_s = 10 N/mm^2, k_s = 26.9 N/mm^2). Additionally, the fully fixed case (k_s = ∞ N/mm^2) was investigated as a reference. The large influence of the support stiffness can be observed from the load-deflection curves at midspan for both FE approaches in Fig. 3a. Compared to the discrete FE approach, the smeared FE approach shows higher stiffness and load

capacity as a result of applying the composite tensile behavior to all Gauss points across the shell thickness. However, the starting branch of the load-deflection curves of both FE models with k_s = 26.9 N/mm^2 shows the correct initial stiffness when compared to the curves obtained experimentally. We also note that the higher the stiffness of the support springs, the smaller the difference between the two FE models, as is evident in the case of the fully fixed shells. This might be attributed to the higher membrane forces in this case (compared to bending stresses), which can be reasonably handled by the smeared model, bringing it closer to the discrete approach.

In addition to the load-deflection curves, the validity of the calculated and used stiffness value (k_s = 26.9 N/mm^2) is evaluated using the relationship between force and support deflection measured experimentally on shell S1-T1R1 in Fig. 3b, which shows close results to the deflections obtained from both FE models for the same shell configuration.

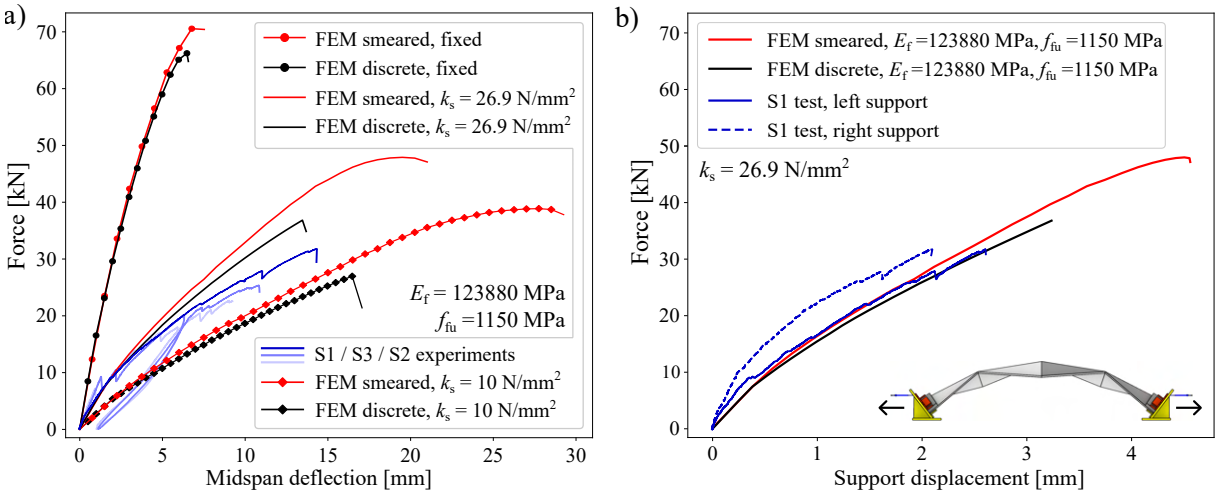

Figure 3: Effect of support stiffness and FEM approach (smeared, discrete) with comparison to experimental data of the 1 cm thick shells: a) load-deflection curves; b) the relation between support displacement and applied load.

3.3 Load-deflection curves and deformations

The load-deflection curves obtained from both FE approaches are provided in Fig. 4 for both shell variants and compared with the equivalent curves from the experiments. Additionally, the results of the discrete model considering the bond law described in Sec. 2.3 for the interface between carbon rovings and concrete are provided in the same figure. While all numerical models correctly capture the initial stiffness of the curves, as expected, the discrete FEM model considering the bond behavior shows the best fit to the experimental data for both shell variants. Therefore, the numerical results in the following will focus on the output of this model.

In addition to the load-deflection curves, the full deformation field in the z direction based on the discrete FEM model with bond effect for one of each shell variant is shown in Fig. 5 and compared with the 3D DIC measurements for the equivalent shell tests. The comparison

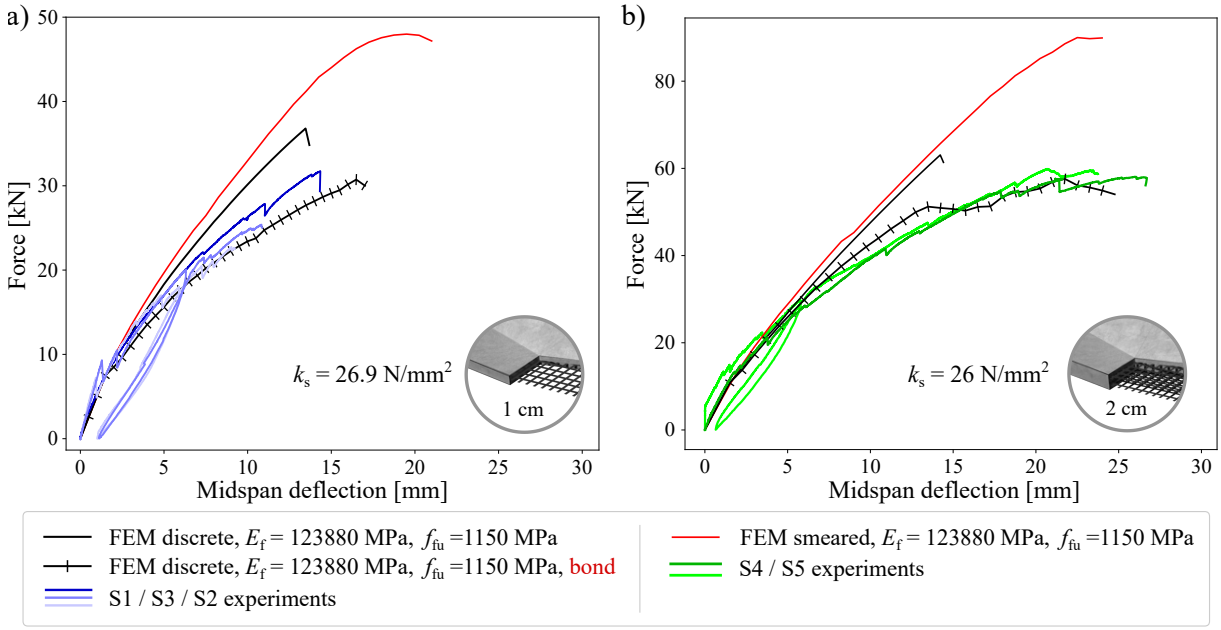

Figure 4: Effect of bond and reinforcement properties on load-deflection curves of FEM analysis compared to experimental data: a) 1 cm thick shells; b) 2 cm thick shells.

confirms the ability of the numerical model to accurately predict both the magnitude and distribution of displacements through the shell.

3.4 Strains and failure modes

The maximum principal strain fields in Fig. 6 are depicted considering the discrete model with and without bond behavior (perfect bond assumption). It can be observed that the model considering the bond behavior displays a strain distribution more aligned with the experimental measurements. Furthermore, the strain at the midspan is remarkably high, corresponding to the presence of two wide cracks on the sides of both shell variants observed experimentally at the same location. In addition, the model without the bond effect (perfect bond) shows a high reinforcement strain on the sides of the shell. The high strains occur because the ideal bond law does not take into account the slipping behavior of the reinforcement. Consequently, the reinforcement is fully activated causing a high strain on the region. It should be noted that both FE models show high localized strain in the vicinity of the supports, which is inconsistent with the experimental DIC data. This is due to the fact that the additional layer of cement mortar applied over the supports to ensure complete fixation was not considered explicitly in the models, but through the described boundary conditions.

The failure modes from all FEM models is due to concrete crushing. In Fig. 7, the minimum principal strain attributed to the failure modes can be seen for both the discrete FE model with bond behavior and the smeared FE model. The local high strain near the supports is irrelevant

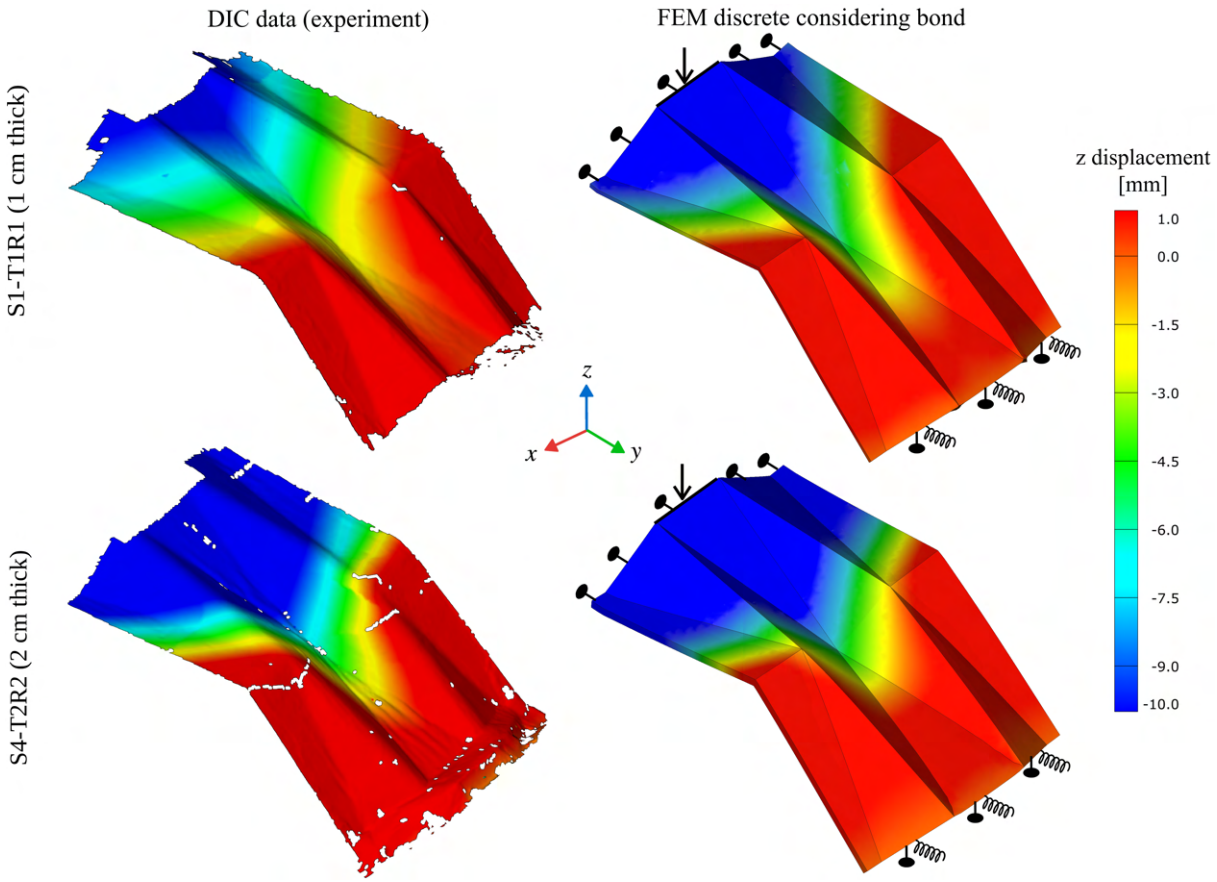

Figure 5: Comparison of the deformed shell geometry at maximum load capacity obtained from DIC data and FEM analysis.

here as previously explained. Also, there is a noticeable compressive strain localization at the sides of the shell at midspan, particularly evident in the smeared model. This strain concentration does not appear in the FE model considering the full shell geometry, as depicted in the top right figure. This strain localization might be attributed to the introduction of symmetry boundary conditions or a mesh deficiency in the reduced shell geometry, but it does not prominently affect the overall structural behavior, e.g., the load-deflection curve. Considering the two mentioned observations, the relevant failure mode observed from both models corresponds well with the experimental observation, which is a failure at the lowest point of the valley to the side of the shell (Fig. 7 top left) in case of the 1 cm thick shells and near the load application point in the middle of the shell (Fig. 7 bottom left) in case of the 2 cm thick shells. Despite overestimating the load capacity, as previously shown, the computationally cheap smeared FE model was able to reasonably provide the correct failure mechanisms of the shells, indicating its suitability for qualitative structural assessment of different folded geometry.

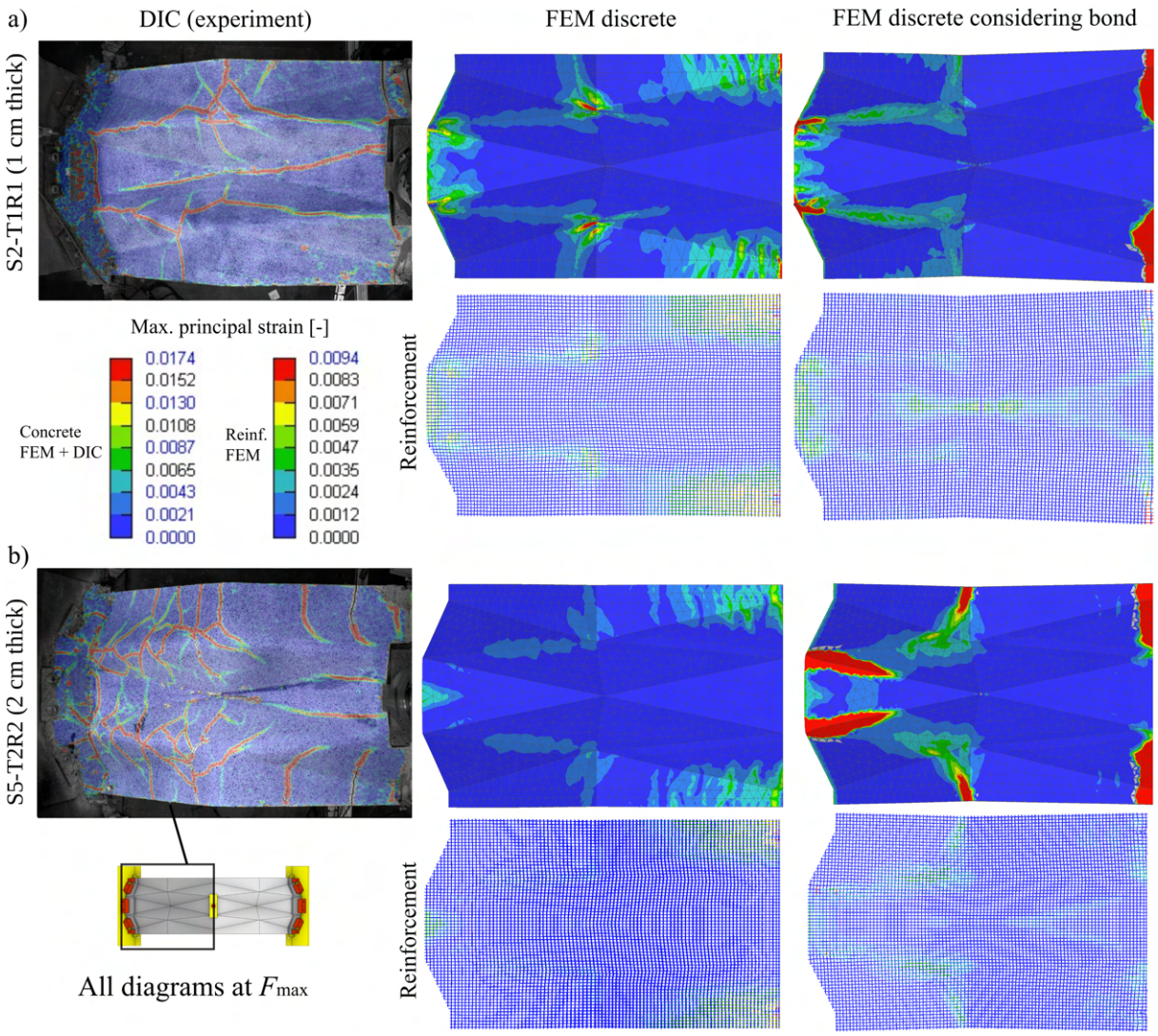

Figure 6: Maximum principal strains of concrete and reinforcement obtained from FEM calculations compared to experimentally obtained DIC measurements; a) 1 cm thick shells with one reinforcement layer; b) 2 cm thick shells with two reinforcement layers.

4 CONCLUSION

In this paper, two modeling strategies based on FE Discrete and FE Smeared methods have been employed to evaluate the structural performance of origami-based carbon reinforced concrete shells. The modeling strategies aim to serve as a basis for the establishment of efficient nonlinear numerical methods that support their design.

The studies indicate that both 2D and 3D elements lead to equivalent results when using the smeared approach. For this reason, opting for 2D elements is advisable due to their superior computational efficiency over 3D elements.

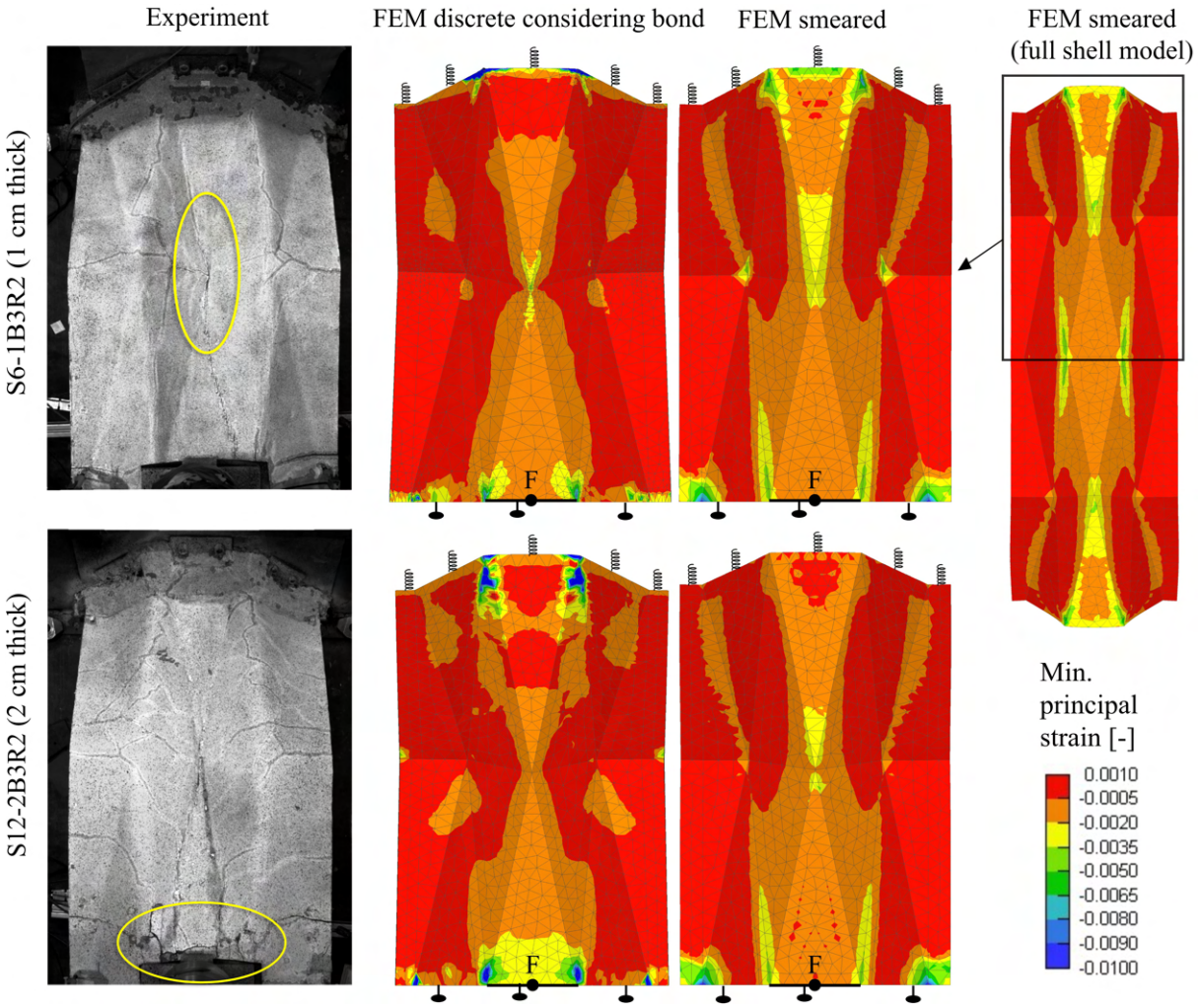

Figure 7: Minimum principal strain obtained from FEM calculations showing the regions with highest compression compared to the compression-induced failure mode observed in the experiments.

The FE smeared, in contrast to the FE discrete, showed an overestimation of the load capacity, probably due to the higher bending stiffness of the assumed shell cross-section with homogeneous tensile behavior. The stiffness of supports significantly affects the structural behavior of the investigated folded shells with low curvature. However, by accounting for the stiffness as springs at both ends of the shell in the models, the load-displacement curves, especially of the discrete model considering bond stress-slip behavior, showed a very good agreement with the curves obtained experimentally.

The displacement magnitude and distribution are correctly predicted by both FE approaches. The maximum principal strain fields is more aligned to the experimental results for the models considering the bond effect of the reinforcement. The models without bond effect (perfect bond assumption) demonstrate strain localization on the sides of the shell due to the fully activation of

the reinforcement in this case. The minimum principal strain fields obtained from both models show the correct failure mechanism for both shell variants, i.e., 1 cm thick with one carbon reinforcement layer and 2 cm thick with two reinforcement layers.

The results of this paper highlights the potential of folded thin-walled carbon textile reinforced concrete elements as both material-efficient and high-performance structural components. It also emphasizes the need to develop computationally efficient nonlinear numerical methods to rapidly and effectively evaluate the structural performance of wide range of geometries offered by waterbomb folding patterns. Folded geometries provide high stiffness and load capacity combined with ease of fabrication, indicating its potential for practical applications. Future research will involve further development of the numerical models to be integrated into a robust and efficient framework for the design of thin, sustainable, and high-performance carbon reinforced concrete elements.

5 ACKNOWLEDGMENT

This work was funded by the Deutsche Forschungsgemeinschaft (DFG, German Research Foundation) – SFB/TRR280, Project-ID 417002380 (C04). The authors acknowledge this support gratefully

REFERENCES

[1] Ajayi, S. O. and Oyedele, L. O. Critical design factors for minimising waste in construction projects: A structural equation modellng approach. *Resources, Conservation and Recycling* (2018) **137**:302-313.

[2] Aveston, J., and Kelly, A. Theory of multiple fracture of fibrous composites. *Journal of Materials Science*. (1973) **8**:352-362.

[3] Červenka, V., Červenka, J. and Pukl, R. ATENA—A tool for engineering analysis of fracture in concrete. *Sadhana.* (2002) **27**:485-492.

[4] Červenka, V., Jendele, L. and Červenka, J. ATENA Program Documentation–Part 1. *Cervenka Consulting sro.* (2021).

[5] Chudoba, R., Niemeyer, A. C., Spartali, H., Robertz, D. and Plesken, W. Description of the origami waterbomb cell kinematics as a basis for the design of thin-walled oricrete shells. *In Proceedings of IASS Annual Symposia (Vol. 2020, No. 23, pp. 1-9).* International Association for Shell and Spatial Structures (IASS). (2020).

[6] Molter, M. *Zum Tragverhalten von textilbewehrtem Beton* (Doctoral dissertation, Aachen, Techn. Hochsch., Diss., 2005). (2005).

[7] Preinstorfer, P., Huber, P., Huber, T., Kromoser, B., and Kollegger, J. Experimental investigation and analytical modeling of shear strength of thin walled textile-reinforced UHPC beams. *Engineering Structures.* (1973) 0141-0296, **231**:352-362.

[8] Robertz, D., Spartali, H., Plesken, W., Chudoba, R. and Niemeyer, A. C. Semi-symmetric origami waterbomb cell kinematics and tessellation for the design of thin-walled folded shells. *In Proceedings of IASS Annual Symposia (Vol. 2022, No. 9, pp. 1-11)*. International Association for Shell and Spatial Structures (IASS). (2022).

[9] Scholzen, A., Chudoba, R. and Hegger, J. Thin-walled shell structures made of textile-reinforced concrete: part I: structural design and construction. *Structural Concrete.* (2015) **6(1)**:106-114.

[10] Sharei, E., Scholzen, A., Hegger, J. and Chudoba, R. Structural behavior of a lightweight, textile-reinforced concrete barrel vault shell. *Composite Structures.* (2017) **171**:505-514.

[11] Spartali, H., Hegger, J. and Chudoba, R. Structural behavior of origami-based folded shells made of carbon textile reinforced concrete. *Universitätsbibliothek der RWTH Aachen.* (2023).

[12] Spartali, H., Woerd, J. D. V. D., Hegger, J. and Chudoba, R. Stress redistribution capacity of textile-reinforced concrete shells folded utilizing parameterized waterbomb patterns. *In Proceedings of IASS Annual Symposia (Vol. 2022, No. 2, pp. 1-11).* International Association for Shell and Spatial Structures (IASS). (2022).

[13] Xu, S., Krüger, M., Reinhardt, H. W., and Ožbolt, J. Bond characteristics of carbon, alkali resistant glass, and aramid textiles in mortar. *Journal of materials in civil engineering.* (2004) **16(4)**:356-364.